Supplementary Information

Fouling-Proof Triple Stream 3D Flow Focusing Based Reactor: Design and Demonstration for Iron Oxide Nanoparticle Co-Precipitation Synthesis

Georgios Gkogkos[a], Maximilian O. Besenhard[a], Liudmyla Storozhuk[c], Nguyen Thi Kim Thanh[b,c], Asterios Gavriilidis[a]

a. Department of Chemical Engineering, University College London, Torrington Place, London WC1E 7JE, UK

b. Biophysics Group, Department of Physics and Astronomy, University College London, Gower Street, London WC1E 6BT, UK

c. UCL Healthcare Biomagnetics and Nanomaterials Laboratories, University College London, 21 Albemarle Street, London W1S 4BS, UK

Contents

1. Preliminary experiments: exploring fouling in simple flow focusing configurations

Fouling was observed during preliminary experiments of IONP co-precipitation with a glass tube-in-tube flow focusing reactor. Fouling occurred almost instantly after starting the reactor, at the confluence point of the reactant streams and was clearly visible only after few seconds (Figure S1 a). Subsequently, agglomerates detached from the wall near the confluence point (Figure S1 b) and attached on the main wall disrupting the flow pattern and accelerating extensive fouling of the reactor (Figure S1 c). While the flow focusing nature of the reactor greatly decelerated fouling, it did not eliminate it. Repeating the synthesis with 10 times lower iron concentration in the core stream slowed down the onset of fouling at the mixing point but did not prevent it eventually.
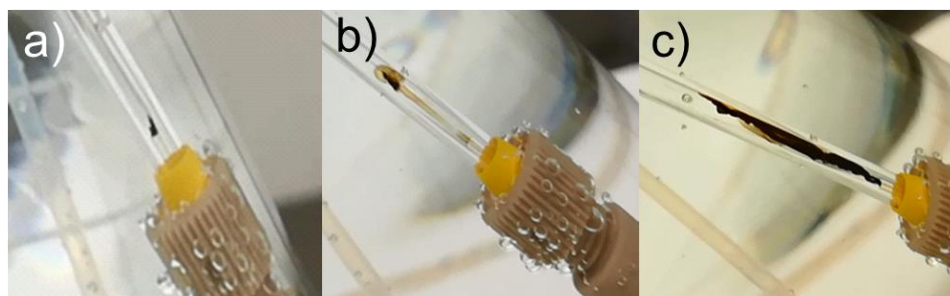

Figure S1: IONP co-precipitation in a tube-in-tube flow focusing reactor. a) Fouling onset at the confluence point, b) detachment of particle agglomerate, c) disruption of flow focusing pattern and fouling on the reactor wall.

Using a rapidly prototyped 2D flow focusing mixer incorporating a separating stream (as described in materials and methods), demonstrated the effectiveness of a separating stream for fouling prevention at the confluence point as seen in Figure S2. Fouling only formed in the outlet channel, away from the confluence point, at the top and bottom channel walls. This experiment also underlined the need for adapting the separating stream principle to a 3D flow focusing device to avoid fouling.

Figure S2: IONP co-precipitation in a 2D flow focusing device with a separating stream (after flushing the device with DI water). Fouling is evident on the top wall of the flow channel.

2. Simulation details of 3D flow focusing geometry

The simulations were setup within COMSOL Multiphysics V5.4. Setup for a given geometry includes selecting the proper physics models and boundary conditions, discretisation of the geometry/simulation domain, solving the resulting system of equations with COMSOL solvers and post processing the results.

2.1 Physics setup

The "Fluid Flow/Laminar Flow" COMSOL module was selected for the whole fluid domain. This solves the Navier-Stokes equations (1) along with the continuity equation (2) for incompressible fluid flow.

$$\rho \frac{\partial \bar{u}}{\partial t} + \rho(\bar{u} \cdot \nabla)\bar{u} = \nabla \cdot [-P\bar{I} + \mu(\nabla\bar{u} + (\nabla\bar{u})^T)] + F \qquad (1)$$

$$\rho\nabla(\bar{u}) = 0 \qquad (2)$$

where ρ is the fluid density, $\bar{u}$ the vector of the velocity, P is the pressure, $\bar{I}$ is the unit vector of the pressure, μ the fluid viscosity and F the external body forces that act on the fluid. The thermophysical properties of water were selected and derived from COMSOL's integrated database. Temperature was set at a constant value of 25 °C which is approximately the room temperature, but since the system only consists of aqueous streams and diffusion is set to be negligible, the resulting flow patterns are temperature independent.

The "tracer" dilute species were introduced via the "Transport of Dilute Species" COMSOL module which solves the mass transport equation in the whole computational domain.

$$\frac{\partial c_i}{\partial t} + \bar{u}\nabla c_i = \nabla(-D\nabla c_i) + R_i \tag{3}$$

where c_i is the concentration of species i, $\bar{u}$ is the vector of the velocity, D the diffusion coefficient of species i and R_i is the generation term of species i. Since no generation (e.g., chemical reaction) was modelled in this system, the generation term was neglected. To mitigate the effect of diffusion and force the tracer to follow the streamlines, the diffusion coefficient of the tracer was set to a very low value ($D = 10^{-20}$ m^2/s).

As boundary conditions, a constant average velocity and a fully developed laminar flow was set at every inlet. In the core inlet the tracer concentration was set as 0.1 M while at the lateral inlet the concentration was set as zero. At the outlet boundary, the relative pressure was set equal to zero and at the walls a no slip condition was assumed. Zero flux was enforced at the walls and at the boundary conditions. Gravity was not included in the simulation, since no significant effect was found during the preliminary experiments with a larger scale tube-in-tube reactor which was tested in various orientations. In addition, no other external body forces were included in the simulations and thus the body force term (F) in equation 1 was neglected.

The average velocities were calculated for given Reynolds numbers from (4)

$$Re = \frac{\rho u D_H}{\mu} \tag{4}$$

where ρ is the fluid density, u the average velocity, μ the fluid viscosity and D_H the hydraulic diameter of each inlet, which for a channel with a cross-sectional area A and wetted perimeter P (A and P refer to the full geometry and not the quarter) is calculated from:

$$D_H = \frac{4A}{P} \tag{5}$$

2.2. Meshing strategy and sensitivity analysis

A structured hexahedral mesh was used in all simulations, since the domain was itself a combination of large hexahedra and can be easily discretised with such elements. The hexahedral (hex) mesh structure also allowed to easily structure the mesh for the needs of the simulation. By introducing high aspect ratio hex-elements, it was possible to refine the areas of interest, such as the initial focusing point in the cross junction, the vicinity of the walls where boundary layers were

expected, and the middle of the main channel where the focused stream of the tracer was expected to form, while retaining a relatively small number of elements along the main channel length. The number of elements was further decreased by introducing a gradual increase in the size of the elements while moving away from the points of interest. Since the gradients of velocity in the direction of the main channel were getting smaller with distance from the mixing point (flow becomes fully developed), the use of elongated elements did not result in significant loss of information. The efficiency of this meshing strategy was tested by solving a test problem with increasingly refined mesh and identified the size that could adequately resolve the physics. The velocity profile (Figure S3 d) in a horizontal line near the mixing point (Figure S3 a) was chosen as an indication of the effect of meshing on hydrodynamics, while the concentration profile (Figure S3 c) was used as means of evaluating the numerical diffusion. Six different meshes were tested on geometry A ranging from 40,000 to 800,000 elements. No significant effect was found on the hydrodynamics as even the coarser mesh (being properly structured) was able to capture the velocity profile adequately. Taking into account the concentration profile as well, mesh M3 (see Fig S4) was chosen as the best compromise, providing enough resolution to qualitatively capture the flow patterns without being overly expensive computationally.
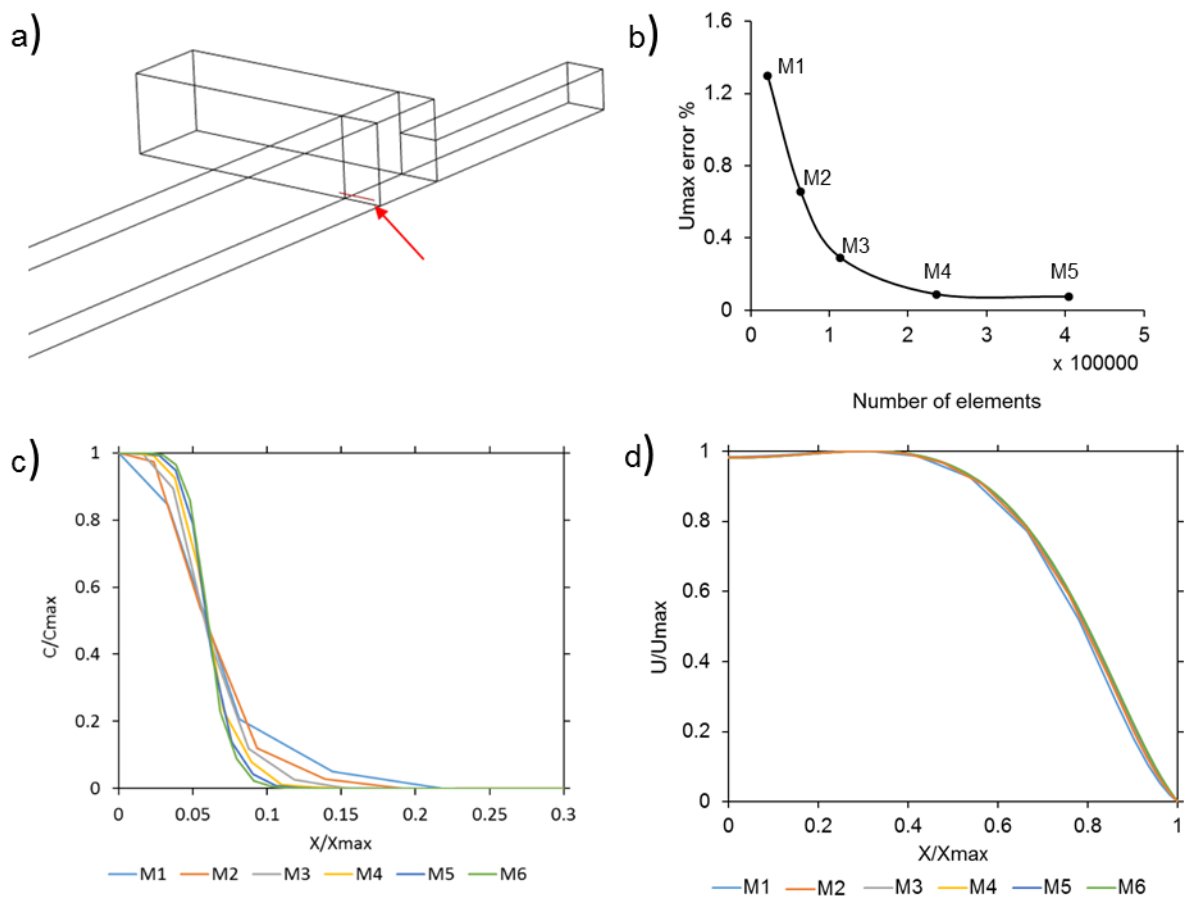
Figure S3: Simulations for mesh sensitivity analysis. a) Linear section near the junction used to evaluate mesh sensitivity. b) Sensitivity % of maximum velocity U_{max} with the total number of elements; M6 did not produce any improvement. c) Concentration profile at the linear section, used for evaluation of numerical diffusion. d) Velocity profile at the linear section used to evaluate meshing effect on hydrodynamic pattern. The x axis in (c) and (d) corresponds to the red line shown in (a).
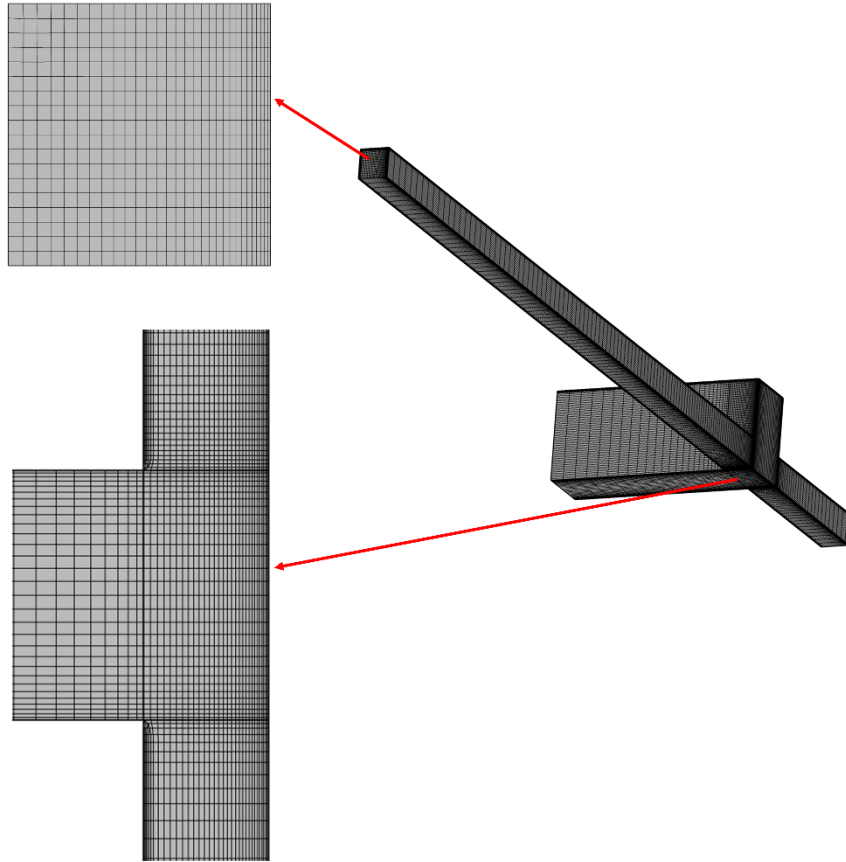
Figure S4: Mesh details of geometry E (see Table 1). Top left: mesh at the outlet, bottom left: mesh at the flow focusing junction.

<u>2.3. Solution strategy</u>

All the simulations were solved in steady state (stationary study selected in COMSOL interface). An iterative approach was chosen in which the solution was generated gradually in multiple iterations instead of a large computational step in the direct approach. This choice greatly reduced the amount of required RAM, allowing to run multiple simultaneous simulations in the same machine. To improve the convergence behavior, an initial solution for each simulation was first obtained by using the coarsest mesh. This solution was then used as the initial value (for velocity and concentration) for the final solution in the structured and refined mesh. This step proved particularly valuable in the high Reynolds number simulations, where the emergence of secondary flows made convergence harder to achieve.

3. Reactor system manufacturing details

3.1. Choice of material

Poly(methyl methacrylate) (PMMA) was the material of choice for the manufacturing of the chip device. PMMA is transparent, allowing optical monitoring of fouling throughout the channel, characterisation of the flow pattern, and it is compatible with a wide range of chemicals, including strong alkaline solutions which wet the channel surface during the chemical synthesis. The highly corrosive iron precursor is in relatively low concentrations (<2% w/w) to avoid damaging the device. In addition to its properties, PMMA is characterised by its ease of machining and well documented bonding processes which facilitates reproducibility in manufacturing of closed channel devices.

3.2. Milling of channels

The milling process was designed according to pre-existing guidelines to ensure satisfactory channel quality and also facilitate the subsequent bonding of the two pieces. The milling depth at each pass was 0.03 mm, ultimately resulting in a total milling depth for each layer of 0.32 mm for the main channel and 1 mm for the lateral channels (total depth for the main channel was 0.64 mm and for the lateral channels was 2 mm resulting in a channel height ratio similar to geometry E in Table 1). The first layer was machined with a smaller depth of 0.02 mm, as this was found to reduce the milling debris' trace on the surface of the device which is critical to achieve proper sealing via bonding of the two parts. The endmill planar velocity was set to 5 mm/s with a rotation frequency of 16,000 rpm. The vertical velocity was set to 2 mm/s. The limits in drill velocity were set to avoid damage of the endmill due to vibrations. The limit in rotation speed also prevents melting of the milled material due to frictional heat dissipation. After milling, the piece was thoroughly cleaned with a soft brush, washed with soap and DI water and dried with filtered compressed air to ensure that no debris or moisture remained inside the channels.

3.3. Solvent assisted thermal bonding

After thorough cleaning of both PMMA layers with commercial detergent and DI water, a thin layer of pure IPA was applied to one of the layers before aligning and clamping them together in steel plates. The steel plates were compressed with threaded steel bolts, to a torque of 4 N·m. The clamped assembly was then placed in a convection oven at 70 ºC for 35 min. After heating, the device was left clamped to cool down to room temperature. Bonding quality was assessed via microscope examination of the channels.

3.4. Assembly of triple stream 3D flow focusing reactor system

For the nanoparticle synthesis, the triple stream 3D flow focusing mixer chip (Figure S5 a) outlet was connected to a 15.4 m long, 1 mm ID PTFE capillary arranged in tight coils of 17 mm diameter. In the room temperature synthesis, a simple straight helical coil configuration was used to better observe the particle stabilisation, while for the high temperature synthesis the capillary was arranged in a square coiled flow inverter configuration (Figure S5 b) to fit in the heating bath container. The hydrodynamics of the two coil configurations are expected to be similar in the operating regime of interest (Reynolds number 8.49-63.7 and Dean number 3.1-10.6)[1]. In the high temperature configuration each inlet was preceded by a 2 m long of 1 mm ID PTFE tubing used for preheating the streams at the required reaction temperature (Figure S5 b). The whole assembly was submerged in a heating stirred water bath (Figure S5 c) for temperature control.
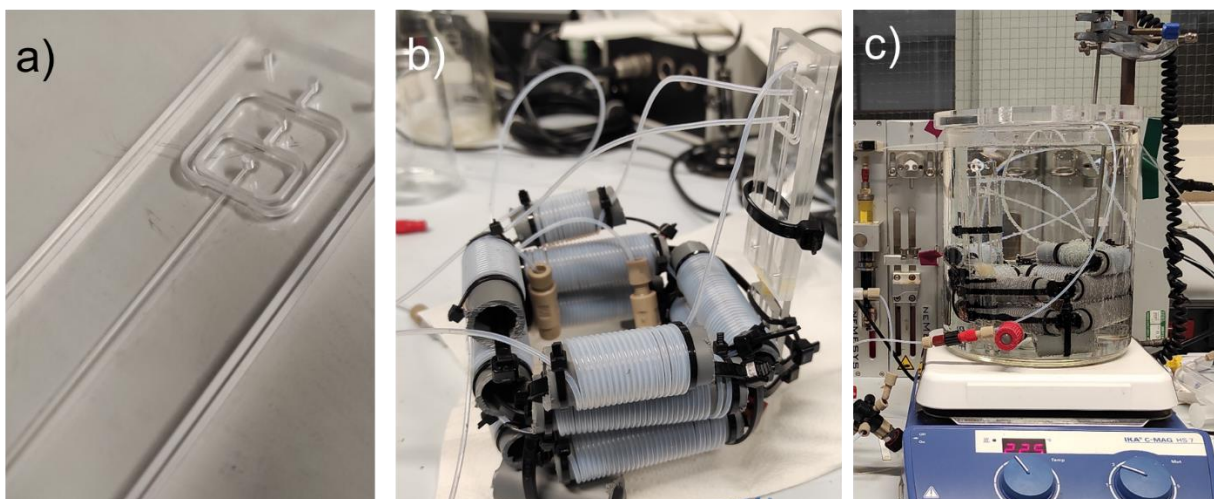

Figure S5: a) The triple stream 3D flow focusing mixer chip made from PMMA, b) integration of the mixer chip with a coiled flow inverter to provide sufficient residence time. Preheating coils precede the inlets of the chip, c) Complete reactor system: The triple stream 3D flow focusing reactor assembly submerged in DI water acting as heating fluid, on a hotplate.

4. Videos of nanoparticle synthesis in the 3D flow focusing reactor assembly

A series of videos accompanying this manuscript show various steps of the particle formation. Videos SV1-SV3 were produced with a non compact version of the reactor, so as to clearly observe various locations:

SV1: IONPs exit the mixer chip focused in the separating stream where they formed. Initial instabilities are evident in the separating stream shortly after it exits that eventually lead to large agglomerate formation.

SV2: Disruption of the focused stream and formation of agglomerates near the beginning of the capillary section.

SV3: Large agglomerates enter the coil section where deagglomeration proceeds at room temperature.

SV4: Fouling at the section between the chip and the capillary coiled flow inverter in a high temperature synthesis with inadequate base concentration.

SV5: Standard operation of a high temperature synthesis with adequate base concentration. Fouling was avoided.

5. Fouling in the triple stream 3D flow focusing mixer chip

Fouling would occur in the triple stream 3D flow focusing mixer when operated below the specified separating stream flowrate. As shown in Figure S6, fouling started at the confluence point and its growth accelerated with occasional agglomerate detachment (as in t = 33 s), before strongly bonding on the wall and requiring cleaning. It should be noted, that even after fouling had occurred, the device could operate again without further fouling growth, if adequate separating stream flowrate was used.
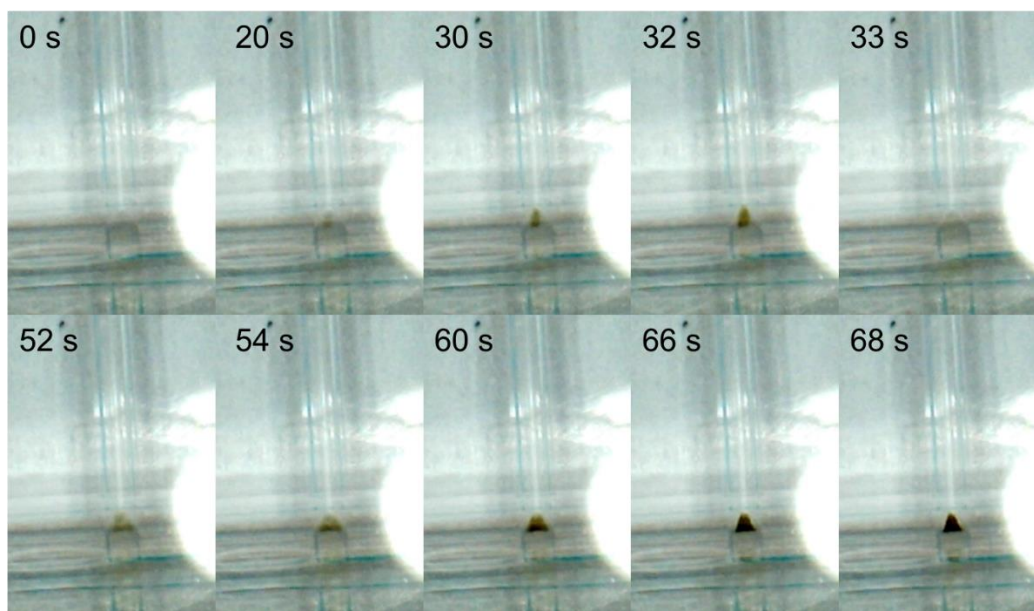
Figure S6: Onset of fouling at the confluence point of the triple stream 3D flow focusing mixer while operating with separating stream flowrate below the minimum required. (Q_{sep} = 0.16 ml/min, Q_{core} = 0.1 ml/min, Q_{TEAOH} = 1 ml/min). Fouling was induced after the separating stream flowrate was reduced to 0.16 from 0.2 ml/min at t = 0.

6. Fouling after the triple stream 3D flow focusing mixer

Fouling was possible downstream of the flow focusing mixer, due to agglomerate formation which deviated from the flow focusing pattern and attached on the capillary wall. Fouling, as shown in Figure S7 (Top), occurred in all cases with lower base concentration or flowrate (Experiments 4-9 and 12-13) with its severity increasing as the base concentration was decreased. In cases where a high base concentration was used, fouling was mitigated throughout the reactor (Figure S7 Bottom). The images in Figure S7 are screenshots from videos SV4 and SV5.
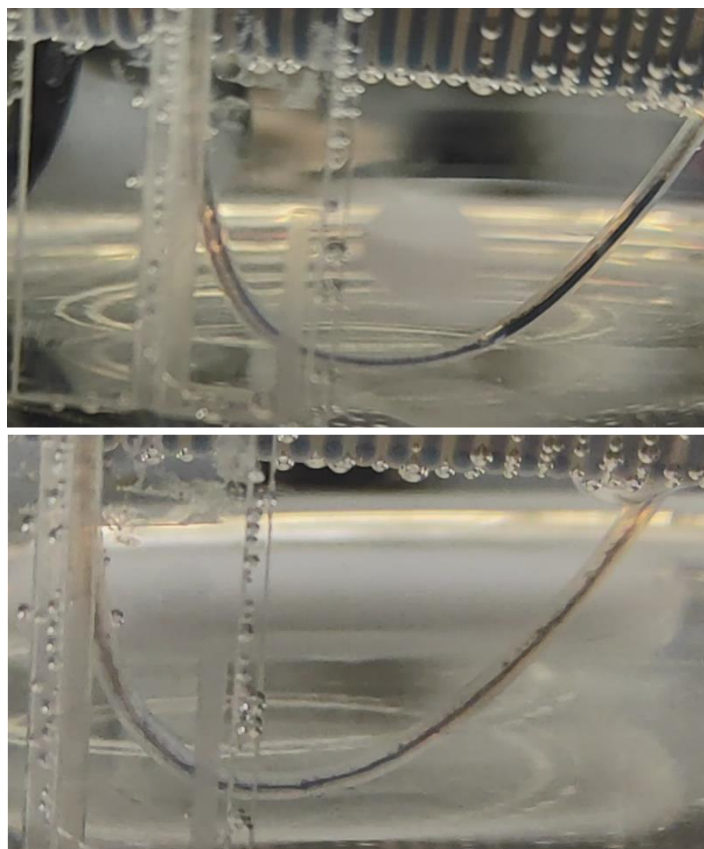
Figure S7: Top: $Q_{TEAOH} = Q_{Fe} = 0.1$ ml/min, $Q_{sep} = 0.6$ ml/min (Experiment 13 in Table 2). Fouling occurred at the first bend after the flow focusing mixer at the capillary connecting the chip mixer with the capillary coiled flow inverter. Bottom: $Q_{TEAOH} = 1$ ml/min, $Q_{Fe} = 0.1$ ml/min, $Q_{sep} = 0.6$ ml/min (Experiment 14 in Table 2). Agglomerates broke-up faster and particles remained in the focused stream before entering the coil section without causing any visible fouling over long time periods. The flow was from left to right along the capillary section shown. The temperature was 60 °C for both cases.

7. References

1.   Rossi, D., Gargiulo, L., Valitov, G., Gavriilidis, A. & Mazzei, L. Experimental characterization of axial dispersion in coiled flow inverters. *Chem. Eng. Res. Des.* **120**, 159–170 (2017).